Cerebral Cortex, January 2018;28: 340–349

doi: 10.1093/cercor/bhx294
Advance Access Publication Date: 9 November 2017
Original Article

ORIGINAL ARTICLE

Amyloid Network Topology Characterizes the Progression of Alzheimer's Disease During the Predementia Stages

Joana B. Pereira[1], Tor Olof Strandberg[2,3], Sebastian Palmqvist[2,4], Giovanni Volpe[5], Danielle van Westen[6,7], Eric Westman[1,†] and Oskar Hansson[2,3,†], for the Alzheimer's Disease Neuroimaging Initiative[‡]

[1]Division of Clinical Geriatrics, Department of Neurobiology, Care Sciences and Society, Karolinska Institute, Stockholm, Sweden, [2]Clinical Memory Research Unit, Department of Clinical Sciences Malmö, Lund University, Lund, Sweden, [3]Memory Clinic, Skåne University Hospital, Malmö Sweden, [4]Department of Neurology, Skåne University Hospital, Sweden, [5]Department of Physics, Göteborg University, Göteborg, Sweden, [6]Department of Clinical Sciences Lund, Diagnostic Radiology, Lund University, Lund, Sweden and [7]Imaging and Function, Skåne University Health Care, Lund, Sweden

Address correspondence to Joana B. Pereira, Department of NVS, Division of Clinical Geriatrics, Novum fifth floor, 141 57 Huddinge, Sweden. Email: joana.pereira@ki.se

[†]Both contributed as senior authors.
[‡]Data used in preparation of this article were obtained from the Alzheimer's Disease Neuroimaging Initiative (ADNI) database (adni.loni.usc.edu). As such, the investigators within the ADNI contributed to the design and implementation of ADNI and/or provided data but did not participate in analysis or writing of this report. A complete listing of ADNI investigators can be found at: http://adni.loni.usc.edu/wp-content/uploads/how_to_apply/ADNI_Acknowledgement_List.pdf

Abstract

There is increasing evidence showing that the accumulation of the amyloid-β (Aβ) peptide into extracellular plaques is a central event in Alzheimer's disease (AD). These abnormalities can be detected as lowered levels of $A\beta_{42}$ in the cerebrospinal fluid (CSF) and are followed by increased amyloid burden on positron emission tomography (PET) several years before the onset of dementia. The aim of this study was to assess amyloid network topology in nondemented individuals with early stage Aβ accumulation, defined as abnormal CSF $A\beta_{42}$ levels and normal Florbetapir PET (CSF+/PET–), and more advanced Aβ accumulation, defined as both abnormal CSF $A\beta_{42}$ and Florbetapir PET (CSF+/PET+). The amyloid networks were built using correlations in the mean ^{18}F-florbetapir PET values between 72 brain regions and analyzed using graph theory analyses. Our findings showed an association between early amyloid stages and increased covariance as well as shorter paths between several brain areas that overlapped with the default-mode network (DMN). Moreover, we found that individuals with more advanced amyloid accumulation showed more widespread changes in brain regions both within and outside the DMN. These findings suggest that amyloid network topology could potentially be used to assess disease progression in the predementia stages of AD.

Key words: amyloid, brain networks, cerebrospinal fluid, florbetapir PET, graph theory

Introduction

Although there is currently no cure for Alzheimer's disease (AD), the past 2 decades have suggested that certain pathological processes may trigger the disease. Amongst these processes, the accumulation of the amyloid-β (Aβ) peptide into extracellular plaques may be a central event that initiates a cascade of synaptic, metabolic and neurodegenerative changes, which ultimately lead to dementia (Jack et al. 2013).

Several studies have assessed Aβ pathology in AD as decreases of $A\beta_{42}$ in the cerebrospinal fluid (CSF) or increased amyloid deposition on positron emission tomography (PET) (Blennow et al. 2015). Although low concentrations of CSF $A\beta_{42}$ are associated with greater amyloid burden on PET imaging (Koivunen et al. 2008; Grimmer et al. 2009; Tolboom et al. 2009; Palmqvist et al. 2014), the agreement between these 2 markers in identifying Aβ pathology is not perfect (Jagust et al. 2009). For instance, previous studies have shown that some individuals may present abnormal CSF $A\beta_{42}$ levels but normal amyloid PET (Mattsson et al. 2015; Palmqvist et al. 2016). This discordant biomarker profile has been found more frequently in subjects that are cognitively normal than in AD patients (Mattsson et al. 2015), suggesting that CSF $A\beta_{42}$ may be an earlier marker of Aβ pathology compared to amyloid PET. Previous findings from our group provide support to this assumption as we found that nondemented cases with abnormal CSF $A\beta_{42}$ levels but normal amyloid PET, showed a higher Aβ accumulation rate than subjects where both modalities were normal, and that was similar to the accumulation rate in subjects with both abnormal CSF and PET (Palmqvist et al. 2016). These results suggest that individuals with abnormal CSF $A\beta_{42}$ levels will eventually develop Aβ pathology also on amyloid PET.

There is increasing evidence suggesting that amyloid plaques are not randomly distributed in the brain but show a characteristic spatial pattern (Braak and Braak 1991). In line with this, amyloid deposition may expand into areas that receive neuronal projections from other brain regions already exhibiting Aβ, spreading between interconnected neurons through large-scale networks (Thal et al. 2002). The organization of the brain as a large-scale network has been extensively assessed in the past few years using concepts from graph theory (Bullmore and Sporns 2009). Using this method, amyloid networks can be built as a collection of nodes representing the mean amyloid values from different brain regions, which are connected by edges corresponding to the links or correlations between them. In a previous study using graph theory analyses, it was shown that Aβ accumulation in the medial temporal lobe is associated with accumulation in medial parietal, orbitofrontal, and temporal areas in individuals with low amyloid burden (Sepulcre et al. 2013). In addition, other studies have also compared the amyloid networks between controls and MCI patients (Jiang et al. 2015; Son et al. 2015) or controls and AD patients (Duan et al. 2017; Jiang et al. 2015; Son et al. 2015). These studies showed network abnormalities in temporal (Son et al. 2015), frontal, parietal (Jiang et al. 2015), or occipital areas (Duan et al. 2017) in the previous patient groups.

To this date, it is not known whether Aβ pathology has a similar impact on the nodal centrality (i.e., number of connections), integration (i.e., critical long-distance connections) or segregation (i.e., local clustering of connections) properties of network organization. Studying the relationship of amyloid deposition between different brain regions is important as it might provide important clues on how Aβ pathology spreads in the brain. In addition, no studies have assessed the amyloid networks in the earliest stages of Aβ accumulation, which can be defined as nondemented individuals with abnormal CSF $A\beta_{42}$ levels but still normal amyloid PET (CSF+/PET−).

Hence, the aim of this study was to assess the organization of the amyloid networks in CSF+/PET− and CSF+/PET+ individuals by combining Florbetapir PET with graph theory. We analyzed measures reflecting centrality, integration and segregation properties in (1) nondemented cases in the earliest stages of Aβ accumulation (CSF+/PET−) and (2) nondemented cases in the more advanced stages of Aβ accumulation (CSF+/PET+). Based on previous evidence showing that several regions with amyloid deposition overlap with the areas of the default-mode network (DMN), (Buckner et al. 2005, 2009; Sperling et al. 2009; Palmqvist et al. 2017), we predicted that CSF+/PET− and CSF+/PET+ subjects would present abnormalities in the DMN. The DMN is a network of interacting brain regions that display highly correlated activity with each other. These regions include the posterior cingulate and precuneus, the medial prefrontal cortex, bilateral angular gyri, and medial temporal lobes (Raichle et al. 2001; Greicius et al. 2004). There is increasing evidence showing that the DMN is involved in different high-level cognitive functions, including day-dreaming, mind-wandering, episodic memory, semantic processing, and attention (Buckner et al. 2008; Mevel et al. 2011). In addition, this network presents abnormalities in predementia stages of AD (Denis and Thompson 2014), suggesting it plays a relevant pathophysiological role in AD-dementia.

Method

Subjects

Data used in the preparation of this article were obtained from the Alzheimer's Disease Neuroimaging Initiative (ADNI) database (adni.loni.usc.edu). The ADNI was launched in 2003 as a public-private partnership, led by Principal Investigator Michael W. Weiner, MD. The primary goal of ADNI has been to test whether serial magnetic resonance imaging (MRI), PET, other biological markers, and clinical and neuropsychological assessment can be combined to measure the progression of mild cognitive impairment (MCI) and early AD.

Our study sample consisted of nondemented individuals who were cognitively normal (CN), presented subjective memory complaints (SMC), early mild cognitive impairment (EMCI) or late MCI (LMCI). Inclusion/exclusion criteria are described in detail at http://www.adni-info.org/. In brief, the included subjects were between the ages of 55 and 90 years, had completed at least 6 years of education, were fluent in Spanish or English, and were free of any significant neurological disease other than AD. These subjects were recruited and assessed across different clinical sites in USA and Canada (for a full list on ADNI's sites, see Weiner et al. 2010). Each site was assigned a principal investigator, a study physician, study coordinator, psychometrist, and a clinical dementia rating (CDR) scale rater. The principal investigator was responsible for overseeing all ADNI-related activities at their site. The study physician was responsible for conducting and supervising the clinical evaluation of all subjects, including physical and neurological examinations, reviewing adverse events and interpreting laboratory results. The psychometrist was in charge of the administration of the ADAS-Cog and the neuropsychological battery of tests, except the CDR scale, which was assessed by an independent rater, as mentioned above. All clinical sites were managed by the ADNI Clinical Core at the University of California (San Diego) and Mayo Clinic (Rochester) (Weiner et al. 2017).

CSF Analysis

CSF collection, processing, and storage procedures have been described previously (Shaw et al. 2009). CSF $A\beta_{42}$ was measured at the ADNI biomarker core (University of Pennsylvania) using the multiplex xMAP Luminex platform (Luminex Corp) with the INNOBIA AlzBio3 kit (Fujirebio).

Amyloid PET

Amyloid deposition was assessed using ^{18}F-florbetapir PET, which was acquired in four 5-min frames 50–70 min after injection of approximately 10 mCi. The 4 frames were coregistered to each other, averaged, interpolated to a uniform image and voxel size ($160 \times 106 \times 96$, 1.5 mm^3), and smoothed to a uniform resolution (8 mm full width at half-maximum). The preprocessed florbetapir data was corregistered to the structural MRI scan, which was preprocessed using FreeSurfer (version 5.3; http://freesurfer.net/) as described elsewhere (Mormino et al. 2009; Landau et al. 2012). The ^{18}F-florbetapir means were extracted from each cortical region included in the Desikan atlas (Desikan et al. 2006) in addition to the hippocampus and amydala (Fischl et al. 2002). In addition, for the current study we calculated a mean standardized uptake value ratio (SUVR) relative to a freesurfer-based reference region consisting of the whole cerebellum, the pons/brainstem region, and eroded cortical white matter (Landau et al. 2015).

Group Classification

Subjects were classified into 4 groups based on CSF $A\beta_{42}$ and ^{18}F-florbetapir PET amyloid markers: normal CSF and PET (CSF–/PET–), abnormal CSF and normal PET (CSF+/PET–), normal CSF and abnormal PET (CSF–/PET+) and abnormal CSF and PET (CSF+/PET+). Subjects with CSF+PET– were in the early Aβ accumulation stages, whereas CSF+PET+ subjects were in more advanced Aβ stages. We established abnormality in CSF $A\beta_{42}$ levels using a previously established cut-off (CSF $A\beta_{42}$: 192 pg/ml) that maximized the separation of autopsy-confirmed AD cases with Aβ pathology from controls without Aβ pathology (Shaw et al. 2009). For ^{18}F-florbetapir PET, abnormal values were defined using the cut-off >0.8724 SUVR, which was established by using mixture modeling statistics to identify an unbiased cut-off. This approach has been used in several previous studies to establish Aβ PET cutpoints (Palmqvist et al. 2014, 2015; Villeneuve et al. 2015).

Network Analysis

In this study, the amyloid networks were built for each group as a collection of nodes representing brain regions connected by edges corresponding to the links between them (He et al. 2007). The nodes were defined using the mean amyloid values from 68 cortical regions of the Desikan atlas in addition to the bilateral hippocampus and amygdala, forming a total of 72 cortical and subcortical regions. The edges were calculated as the partial correlation coefficients using Pearson's R between every pair of brain regions, while controlling for the effects of age, gender, education, apolipoprotein (*APOE*) ε4 carriership, and diagnosis.

This procedure provides a very convenient and structured way of analyzing the topology of amyloid pathology and its spread. Of note, the edges or connections between brain regions in amyloid PET networks have a different interpretation compared with networks derived from diffusion tensor imaging (DTI) or functional magnetic resonance imaging (fMRI). In a DTI network, 2 regions are connected if there is a physical white matter tract uniting them. In a fMRI network, 2 regions are considered to be connected if their BOLD signals correlate with each other, showing a synchronous pattern of brain activation across time. In contrast, in an amyloid network, 2 regions are considered to be connected if their amyloid values correlate with each other, which occurs when 2 regions show a similar number of plaques or amyloid deposition.

In this study, for each group, we generated a weighted association matrix by compiling all pairwise associations in mean amyloid values between the nodes of each group. To compare network topology between the groups, these matrices were binarized (He et al. 2007) using a range of network densities D to ensure all groups had the same number of edges: D_{min} = 5% to D_{max} = 15%, in steps of 0.3%. For densities below 5%, the number of edges was inferior to the number of nodes, corresponding to a widely disconnected network. For D above 15%, the networks became similar to random graphs and showed a small-world index close to 1. All self-connections were excluded from the analyses.

Network topology can be assessed using a variety of measures that characterize the importance of the nodes in a network (centrality), the ability to combine information between distant brain regions or global efficiency (integration) and the capacity for specialized processing within densely interconnected groups of regions (segregation) (Rubinov and Sporns 2010). In this study, we assessed centrality by calculating the nodal degree, which is the number of connections that link a node to the rest of the network (Rubinov and Sporns 2010). We assessed the integration of the network using the global efficiency, which is the average inverse of the shortest path length between a node and the rest of the network (Latora and Marchiori 2001). Note that the global efficiency for a given node is different from the local efficiency, another commonly used measure in graph theory analyses. The local efficiency assesses the shortest path length between 1 node and its immediate neighbors, whereas the global efficiency assesses the shortest path length between 1 node and all the other nodes in the network (Rubinov and Sporns 2010). We assessed network segregation by calculating the nodal clustering coefficient, which quantifies the number of connections that exist between the nearest neighbors of a node as a proportion of the maximum number of possible connections (Watts and Strogatz 1998). Finally, in this study, we also assessed the community structure by carrying out a modularity analysis, which subdivided the whole-brain amyloid network into groups of nodes, with a maximally possible number of within-group links and a minimally possible number of between-group links (Newman 2004). Figure 1 provides a schematic overview of the analysis of amyloid networks carried out in the current study.

The construction of brain networks and graph theory analyses were performed using BRAPH (Brain analysis using grAPH theory; http://braph.org/; Mijalkov et al. 2017).

Statistical Analysis

To assess differences between groups in demographic, clinical, genetic, and amyloid variables, we carried out nonparametric tests between every pair of groups using Mann-Whitney U tests and Chi-squared tests due to the non-normal distribution of the data. To establish Aβ PET cutpoints, finite mixture models were carried out using the mixtools package of R (R Foundation for Statistical Computing, Vienna, Austria, 2013; version 3.2.2).

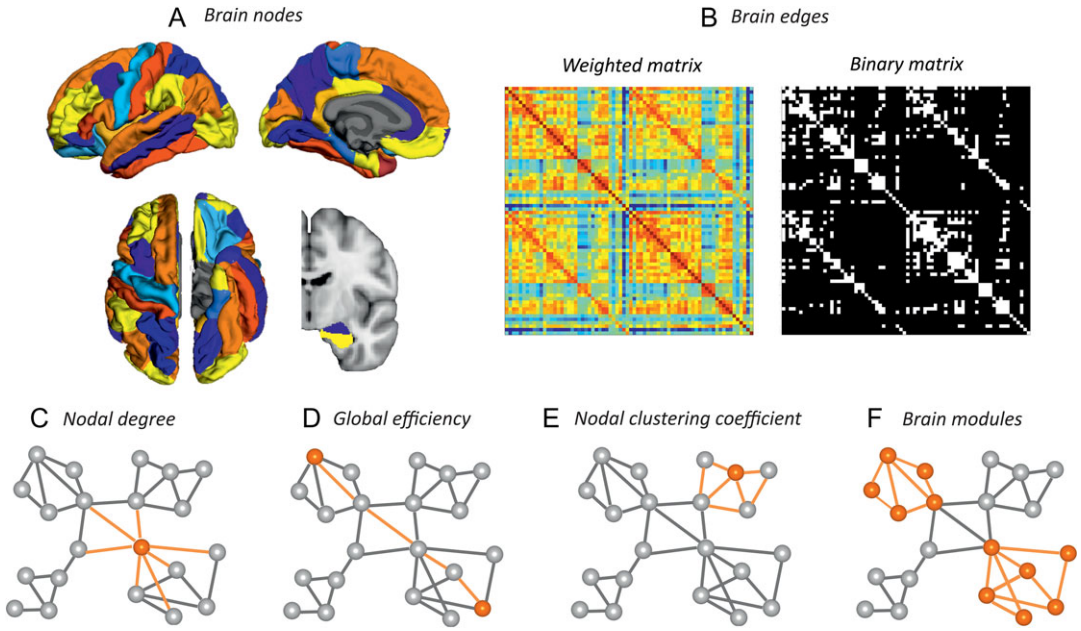

Figure 1. Overview of the methodology. Amyloid networks were built as a set of nodes connected by edges. The nodes were defined as the mean amyloid values extracted from 72 cortical and subcortical brain regions (A), whereas the edges were calculated using partial correlation Pearson's R, which were included in a weighted connectivity matrix (B). This matrix was binarized using a range of densities (B) and the nodal degree (C), global efficiency (D), nodal clustering coefficient (E) and brain modules (F) were computed and compared between groups.

To assess the statistical significance of the differences in the network measures between groups, we carried out nonparametric permutation tests with 1000 replicates (Bassett et al. 2008; He et al. 2008). First, the nodal degree, global efficiency and nodal clustering coefficient were calculated separately for each group. Then, we randomly reallocated each subject's set of regional amyloid values to one of the groups and computed the partial correlation matrices for each randomized group. These matrices were binarized using the same range of densities as in the real networks and we calculated the differences in network measures between the randomized groups for each network density. This randomization procedure was repeated 1000 times and the 95th confidence intervals were used as the critical values for a 2-tailed test at $P < 0.05$. A false discovery rate (FDR) correction (Benjamini and Hochberg 1995) was applied across the 72 brain regions to control for multiple comparisons ($q < 0.05$). Below, we present the significant nodal results after FDR corrections at $D = 10.1\%$, which corresponds to the middle value in the density range assessed in the current study (5–15%, in steps of 0.3%). However, the mean nodal values, 95th confidence intervals and *P*-values obtained for the group comparisons across all other network densities evaluated in this study have been included in Supplementary Material (Supplementary Tables 1, 2 and 3).

Results

Our sample consisted of 651 subjects, who were classified into different groups based on CSF $A\beta_{42}$ and ^{18}F-florbetapir PET amyloid markers. Hence, 291 subjects were classified as CSF $A\beta_{42}$ negative and ^{18}F-florbetapir PET negative (CSF−/PET), 81 subjects as CSF $A\beta_{42}$ positive and ^{18}F-florbetapir PET negative (CSF+/PET−), 7 subjects as CSF $A\beta_{42}$ negative and ^{18}F-florbetapir PET positive (CSF−/PET+) and 272 subjects as CSF $A\beta_{42}$ positive and ^{18}F-florbetapir PET positive (CSF+/PET+). The characteristics of this sample can be found in Table 1.

Compared to the CSF−/PET− group, CSF+/PET− subjects showed a higher prevalence of the *APOE* ε4 allele ($P < 0.001$).

Compared to both the CSF−/PET− and CSF+/PET− groups, CSF+/PET+ subjects were significantly older ($P < 0.001$, $P = 0.003$), less educated ($P = 0.036$, $P = 0.019$), had more LMCI and less CN or SMC subjects ($P < 0.001$, $P < 0.001$), worse MMSE scores ($P < 0.001$, $P < 0.001$) and a higher prevalence of the *APOE* ε4 allele ($P < 0.001$, $P < 0.001$).

The regional amyloid values in each group are displayed in Supplementary Figure 1. These values show that the distribution of amyloid in the brain did not follow a random pattern, in line with previous evidence showing the progressive and continuous nature of amyloid pathology (Vlassenko et al. 2011; Sepulcre et al. 2013; 2016) in specific sets of brains regions (Palmqvist et al. 2017).

Below, we describe the quantitative differences in network analyses between the CSF−PET− and CSF+PET− groups and between the CSF+PET− and CSF+PET+ groups. We did not carry out analyses in the CSF−/PET+ group due to small sample size ($n = 7$). Comparisons between the CSF−PET− and CSF+PET+ groups have been included in Supplementary Material (Supplementary Fig. 2, Supplementary Table 1).

Nodal degree

We found that the early Aβ accumulation group (CSF+/PET−) showed a higher nodal degree in several brain regions compared to CSF−/PET− (Fig. 2, Supplementary Table 2). These regions were mostly located in the medial brain surface and included the medial orbitofrontal, rostral anterior cingulate, caudal anterior cingulate, posterior cingulate, and isthmus cingulate in addition to the insula and parahippocampal gyri. Moreover, there were also decreases in the nodal degree in the CSF+/PET− subjects when compared to CSF−/PET− in the bilateral postcentral and right precentral gyri.

Table 1. Characteristics of the sample.

	CSF−/PET− (n = 291)	CSF+/PET− (n = 81)	CSF−/PET+ (n = 7)	CSF+/PET+ (n = 272)	CSF−/PET− vs CSF+/PET− (p value)	CSF−/PET− vs CSF−/PET+ (p value)	CSF−/-PET − vs CSF+/PET+ (p value)	CSF+/PET− vs CSF+/PET+ (p value)
Age (years)	71.2 (55.5–89.6)	71.7 (55.0–91.4)	75.3 (67.8–88.3)	74.3 (55.0–87.8)	0.598	0.119	<0.001	0.003
Sex (m/f)	144/147	37/44	5/2	130/142	0.544	0.255	0.688	0.688
Education (years)	17 (8–20)	17.0 (12–20)	15.4 (12–20)	16 (10–20)	0.332	0.248	0.036	0.019
CN/SMC/EMCI/ LMCI	96/49/110/36	30/9/28/14	2/5/0/0	42/18/107/105	0.398	0.262	<0.001	<0.001
MMSE	29 (24–30)	29 (24–30)	27.1 (23–30)	28 (21–30)	0.628	0.091	<0.001	0.001
APOE ε4 (%)	18.6%	48.1%	28.6%	63.6%	<0.001	0.487	<0.001	<0.001
CSF $A\beta_{42}$ (ng/L)	230.4 (192.1–321.5)	167.4 (99.2–191.1)	209.2 (193.2–236.7)	135.2 (84.7–189.6)	<0.001	0.009	<0.001	<0.001
Global ^{18}F-florbetapir PET SUVR	0.73 (0.6–0.9)	0.79 (0.7–0.9)	0.92 (0.9–1.0)	1.14 (0.9–1.5)	<0.001	<0.001	<0.001	<0.001

Values represent medians followed by range, unless otherwise specified. Differences between groups were assessed using Mann–Whitney U or Chi-squared tests. CSF−/PET−, subjects with normal CSF Aβ42 and ^{18}F-florbetapir PET; CSF+/PET−, subjects with abnormal CSF Aβ42 and normal ^{18}F-florbetapir PET; CSF−/PET+, subjects with normal CSF Aβ42 and abnormal ^{18}F-florbetapir PET; CSF+/PET+, subjects with abnormal CSF Aβ42 and ^{18}F-florbetapir PET.

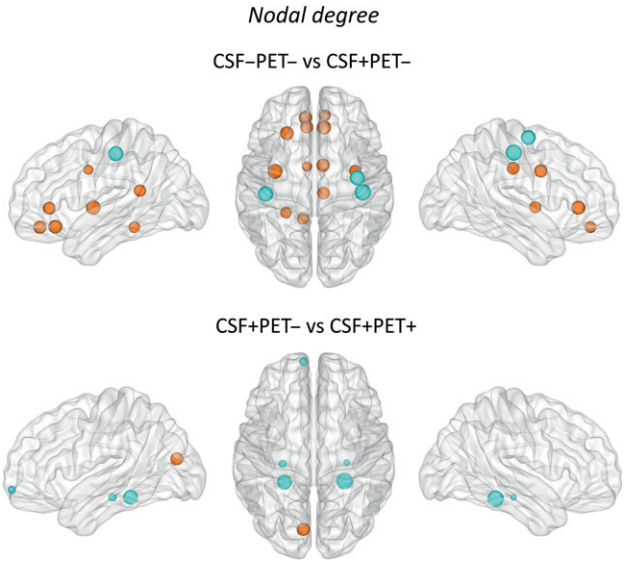

Figure 2. Differences between groups in the nodal degree. The regions showing significant nodal degree increases are colored in orange, whereas the regions showing nodal degree decreases are colored in blue. These regions are listed in Supplementary Tables 2 and Table 3. Larger nodes indicate greater differences between groups. CSF−/PET−, subjects with normal CSF $A\beta_{42}$ and ^{18}F-florbetapir PET; CSF+/PET−, subjects with abnormal CSF $A\beta_{42}$ and normal ^{18}F-florbetapir PET; CSF+/PET+, subjects with abnormal CSF $A\beta_{42}$ and ^{18}F-florbetapir PET.

When we compared the early and more advanced Aβ accumulation groups with each other, we found that the more advanced Aβ group (CSF+/PET+) showed a higher nodal degree in the left cuneus and a lower nodal degree in the left frontal pole, bilateral hippocampus and parahippocampal gyri compared to the early Aβ group (CSF+/PET−) (Fig. 2, Supplementary Table 3).

Global efficiency

We found that that the early Aβ (CSF+/PET−) subjects showed increases in the global efficiency mostly in medial (medial orbitofrontal, rostral anterior cingulate, caudal anterior cingulate, posterior cingulate, isthmus cingulate, precuneus) and temporal (hippocampus, transverse temporal, insula, parahippocampal gyri) brain regions as well as a few frontal areas (superior frontal, pars opercularis) (Fig. 3, Supplementary Table **2**) compared to the CSF−/PET− group.

The comparison of the early and more advanced Aβ accumulation groups showed that the later Aβ group (CSF+/PET+ subjects) had global efficiency increases in the left cuneus and efficiency decreases in the bilateral hippocampus and parahippocampal gyri compared to the early (CSF+/PET−) group, similarly to the results we found for the nodal degree (Fig. 3, Supplementary Table 3).

Nodal clustering coefficient

We found that the CSF+/PET− subjects showed clustering decreases in the bilateral supramarginal and right lateral occipital gyri (Fig. 4, Supplementary Table 2) compared to the CSF−/PET− group.

The comparison of the early and later Aβ accumulation groups showed clustering increases in the left pericalcarine gyrus in the CSF+/PET+ group compared to the CSF+/PET− subjects (Fig. 4, Supplementary Table 3).

Modularity Analysis

We identified 2 modules in the CSF−PET−, CSF+PET− and CSF+PET+ groups (Fig. 5). For a full list of the regions that belong to each module, see Supplementary Table 4.

In the CSF−PET− group, Module I included medial brain areas such as the medial orbitofrontal gyrus, rostral anterior cingulate, caudal anterior cingulate, posterior cingulate, isthmus cingulate, and precuneus.

In the CSF+PET− group, Module I included the previous brain areas in addition to a few temporal and parietal regions such as the superior temporal, transverse temporal, and supramarginal gyri.

In the CSF+PET+ group, Module I also included the same medial brain areas in addition to several frontal and parietal regions such as the rostral middle frontal, lateral orbitofrontal, superior parietal, and inferior parietal gyri.

Module II was mainly composed of lateral occipital and lateral temporal regions in all groups. In addition, it also included lateral frontal regions in the CSF−PET− and CSF+PET− groups.

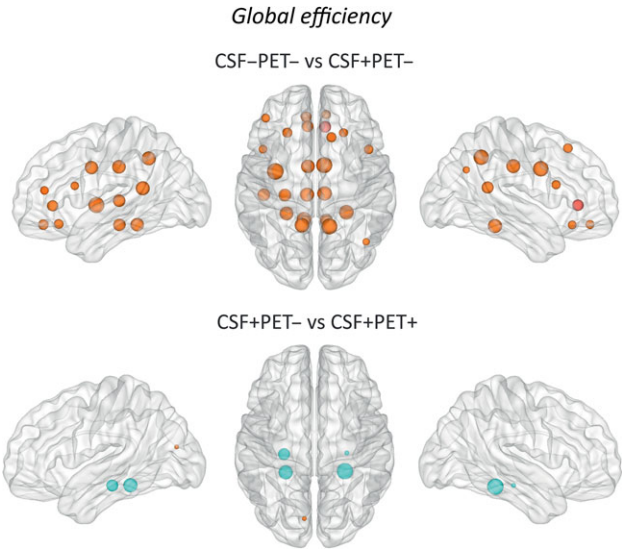

Figure 3. Differences between groups in the global efficiency. The regions showing significant global efficiency increases are colored in orange, whereas the regions showing nodal degree decreases are colored in blue. These regions are listed in Supplementary Tables 2 and Table 3. Larger nodes indicate greater differences between groups. CSF–/PET–, subjects with normal CSF $A\beta_{42}$ and ^{18}F-florbetapir PET; CSF+/PET–, subjects with abnormal CSF $A\beta_{42}$ and normal ^{18}F-florbetapir PET; CSF+/PET+, subjects with abnormal CSF $A\beta_{42}$ and ^{18}F-florbetapir PET.

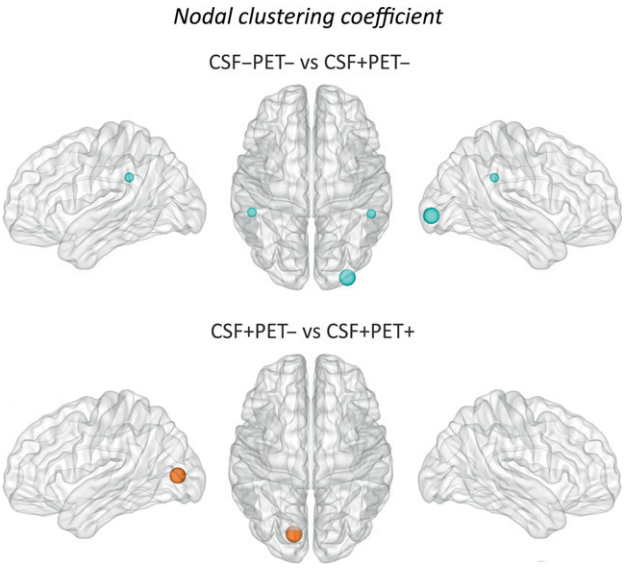

Figure 4. Differences between groups in the nodal clustering coefficient. The regions showing significant nodal clustering coefficient increases are colored in orange, whereas the regions showing nodal degree decreases are colored in blue. These regions are listed in Supplementary Tables 2 and 3. Larger nodes indicate greater differences between groups. CSF–/PET–, subjects with normal CSF $A\beta_{42}$ and ^{18}F-florbetapir PET; CSF+/PET–, subjects with abnormal CSF $A\beta_{42}$ and normal ^{18}F-florbetapir PET; CSF+/PET+, subjects with abnormal CSF $A\beta_{42}$ and ^{18}F-florbetapir PET.

Discussion

In this study, we assessed the organization of amyloid networks in nondemented individuals with abnormal early and late markers of Aβ pathology. Our findings showed an association between the very early accumulation of Aβ fibrils with an increased covariance and shorter paths between several brain areas that overlapped with the DMN. Moreover, we found that nondemented individuals with more advanced amyloid pathology showed changes both within and outside the DMN compared to early amyloid accumulators. Altogether, these findings suggest that the pattern of network changes is different in the earliest and later stages of Aβ pathology and could potentially be used to assess disease progression in the predementia stages of AD.

The hypothesis that Aβ has a causal role in the pathogenesis of AD has received support from different lines of evidence, including the early accumulation of amyloid in the brain in people who go on to develop sporadic AD (Palop and Mucke 2016). This amyloid accumulation starts with the formation of non-fibrillar Aβ species, which results in decreased CSF $A\beta_{42}$ levels but cannot be detected with amyloid PET (Fagan et al. 2009; Morris et al. 2010). Only when these non-fibrillar Aβ species become fibrillar and form neuritic plaques, amyloid PET scans become abnormal, but not earlier in the disease process (Mathis et al. 2012).

In the current study, we found that a group of nondemented subjects presented lowered CSF $A\beta_{42}$ levels but normal amyloid PET, consistent with previous findings showing that an earlier stage of Aβ accumulation may be present in the course of AD. These individuals (CSF+/PET–) showed network abnormalities that were mainly characterized by an increased nodal degree and higher global efficiency. The nodal degree increases were observed in the anterior cingulate, posterior cingulate, medial orbitofrontal gyri, and parahippocampus. The global efficiency increases were observed in the previous brain areas in addition to the precuneus, hippocampus, isthmus cingulate, lateral frontal, and parietal regions. Altogether, these regions appear to overlap with a set of heteromodal high-order association areas that belong to the DMN (Raichle et al. 2001; Greicius et al. 2004), in line with our initial hypothesis.

In contrast to the nodal degree and global efficiency, the clustering coefficient showed relatively few changes in CSF+PET– individuals. In the amyloid network, increases in nodal network measures occur when regions that are affected by Aβ pathology to a similar extent co-vary with each other (nodal degree), have shorter network paths (global efficiency), or form clusters with nearby areas (nodal clustering coefficient). The fact that more prominent changes were found in the degree and global efficiency in early Aβ accumulators (CSF+PET– subjects) could have a biological interpretation related to the DMN, where most of our results were observed. Previous findings have shown that many regions of the DMN have a higher number of connections compared to other brain areas, especially those located along the parasagittal line, such as the medial prefrontal cortex and precuneus (van den Heuvel and Sporns 2013). In addition, the regions that belong to the DMN are relatively far away from each other compared with regions that belong to other networks, such as the precentral and postcentral areas of the sensorimotor network. This implies that short paths exist between the distant regions of the DMN; otherwise they would not be able to efficiently communicate with each other. Thus, the high number of connections and short network paths that characterize the regions of the DMN make them ideal candidates as epicenters of the brain through which disease proteins may initially spread to other areas (Zhou et al. 2012). Our results provide support to this assumption since we found a higher degree and global efficiency between the regions of the amyloid network that overlapped with the regions of the DMN. The relatively few changes we found in the clustering

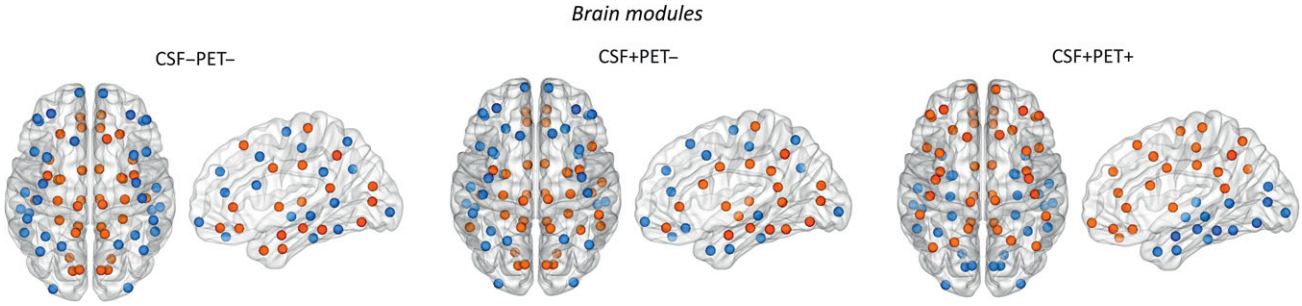

Figure 5. Brain modules in the different groups. We identified two modules in each group. For a full list of regions that belonged to each module, see Supplementary Table 4. CSF–/PET–, subjects with normal CSF $A\beta_{42}$ and ^{18}F-florbetapir PET; CSF+/PET–, subjects with abnormal CSF $A\beta_{42}$ and normal ^{18}F-florbetapir PET; CSF+/PET+, subjects with abnormal CSF $A\beta_{42}$ and ^{18}F-florbetapir PET.

coefficient fit well with this view and with the findings of a recent study (Sepulcre et al. 2016) suggesting that early Aβ deposits may not affect local neighboring areas (clustering) to the same extent as distant brain regions (global efficiency) in early stages of amyloid accumulation.

When the early Aβ accumulators (CSF+/PET– subjects) were compared to the more advanced Aβ accumulators (CSF+/PET+ subjects), we found again significant differences in the nodal degree and global efficiency in addition to one change in the nodal clustering. These differences were characterized by increases in network measures in the parahippocampal gyri and hippocampus in the CSF+/PET– group and increases in occipital areas such as the left pericalcarine gyrus and cuneus in the CSF+/PET+ group. The increases observed in the parahipppocampal gyri and hippocampus in CSF+/PET– subjects are in line with previous evidence suggesting that Aβ may initially expand from these brain areas to other brain regions at very early stages of amyloid accumulation (Sepulcre et al. 2013). These areas may make an essential contribution to the neurodegeneration process first by intraneuronally accumulating neurofibrillary tangles and second by extraneuronally inducing amyloid deposition in its synaptic terminals of projecting neurons (Pearson and Powell 1989). Hence, they might be useful to distinguish early and late stages of amyloid burden. The increases we observed in occipital areas in CSF+/PET+ subjects suggest that areas falling outside the DMN might signal the spread of connectivity abnormalities to other neocortical regions, reflecting the progression of the disease in later amyloid stages.

The resolution of the PET scans that were used to build the amyloid networks in the current study did not allow contrasting our findings directly with the stages of amyloid deposition or neurofibrillary tangles provided by Braak and Braak (1991) since these include very small brain structures such as the basal forebrain nuclei, substantia nigra or hippocampal subfields. However, in general, we found that the early Aβ accumulators (CSF+/PET– subjects) showed network changes consistent with the intermediate amyloid stages proposed by Braak and Braak (1991), in which pathological abnormalities are found in almost all neocortical association areas. In addition, the late Aβ accumulators (CSF+/PET+ subjects) showed network changes that were in line with late amyloid stages (Braak and Braak 1991), in which amyloid deposits spread from the previous areas to primary sensory and motor regions such as the pericalcarine and paracentral gyrus (Supplementary Fig. 2 and Supplementary Table 1). Hence, our network findings in early and later Aβ accumulators were in line with the intermediate and late neuropathological stages of amyloid deposits in AD (Braak and Braak 1991). Regarding the distribution of neurofibrillary tangles, our findings in early and late Aβ accumulators showed some agreement with the later stages of tau pathology, in which tangles are found in isocortical areas (Braak and Braak 1991).

The modularity analyses carried out in the current study revealed the existence of 2 communities of nodes in the amyloid networks across all groups. One of these communities included several regions that belong to the DMN such as the anterior cingulate, posterior cingulate and precuneus. This subnetwork was present in all groups but included additional lateral temporal and parietal areas in CSF+PET– subjects as well as additional lateral frontal and parietal areas in CSF+PET+ subjects. Previous studies have shown that regions from the lateral temporal, parietal, and frontal lobes show increased amyloid deposition on PET in cognitively normal and mild cognitive impairment subjects who have a positive amyloid scan (Pike et al. 2007; Forsberg et al. 2008). These areas, especially the ones in the frontal lobes, show more prominent amyloid pathology in nondemented subjects with cognitive deficits who later convert to AD (Okello et al. 2009). Hence, our findings of a subnetwork that extended from medial brain areas in CSF–PET– subjects to lateral and more widespread brain regions in CSF+PET– and CSF+PET+ individuals is in line with previous studies showing the regional spread of amyloid pathology with progression to AD.

Although the amyloid cascade hypothesis, which posits that Aβ accumulation is the key event leading to neurodegeneration (Jack et al. 2010), has dominated the AD field for the past years (Chetelat 2013), a few studies have highlighted inconsistencies with the linear structure of this hypothesis. For instance, Knopman et al. (2013) showed that the initial appearance of neurodegeneration markers in cognitively normal individuals may be independent of amyloid pathology. Moreover, subjects carrying the *APOE* e4 allele, who are at increased risk of developing sporadic AD, can show Aβ-independent reduced glucose metabolism (Jagust and Landau 2012). Although these findings are not in line with the amyloid cascade hypothesis, there is strong evidence showing that individuals with amyloidosis present a greater risk of developing AD and show AD-related brain abnormalities (Pike et al. 2007; Okello et al. 2009; Vlassenko et al. 2011; Landau et al. 2012; Musiek and Holtzman 2015). The network changes we observed in the areas of the DMN in CSF+PET– and CSF+PET+ subjects provide further support to the role of amyloid in AD as the DMN is typically disrupted in these patients (Buckner et al. 2005, 2009).

Despite the value of our study in characterizing disease progression, a few limitations should be recognized. First of all, although partial volume corrections were carried out, we

cannot exclude the possibility that nonspecific amyloid binding could have influenced some of our network findings. Second, the cross-sectional design of our study is also a limitation since amyloid progression should be assessed by analyzing amyloid accumulation over time. Finally, the assessment of network topology we carried out does not allow performing correlations with clinical measures since we did not have a network for each subject but only a network per group. This limitation has been previously assessed in the analysis of structural MRI networks by Tijms et al. (2012, 2016) and needs to be addressed in future graph theory studies for 3D PET imaging.

In conclusion, our study assessed amyloid network topology in individuals with abnormal CSF $A\beta_{42}$ levels and normal/abnormal amyloid PET using 3 network measures: nodal degree, global efficiency, and clustering coefficient. The interpretation of the results associated with the nodal degree was relatively straightforward; regions with similar amyloid values correlated with each other and showed strong co-variance. In contrast, the interpretation of the global efficiency and clustering coefficient results in an amyloid PET network was less straightforward. The global efficiency provides an insight on the correlations in amyloid values between brain regions that are far away from each other. We found that this measure was increased in the CSF+PET− and CSF+PET+ subjects, suggesting that distant brain regions showed similar amyloid values. On the other hand, the nodal clustering coefficient provides an insight on the correlations in amyloid values between brain regions that are close to each other. We found that this measure detected fewer changes in CSF+PET− and CSF+PET+ subjects, suggesting that, in general, neighboring brain regions did not show similar amyloid values. Hence, the global efficiency seems to be more relevant in characterizing network changes in early and later amyloid accumulators, indicating that distant brain areas correlate in their amyloid values and might act as conduits of propagation of Aβ pathology. Regarding the localization of network changes, we found that subjects with early amyloid pathology showed increases in the nodal degree and global efficiency in regions that overlapped with the DMN. In contrast, subjects with advanced amyloid pathology showed changes in areas both within and outside the DMN compared to early Aβ accumulators. Altogether, our findings contribute to an increased understanding on the mechanisms of Aβ pathology and could provide a novel approach for the early detection of the predementia stages of AD.

Supplementary Material

Supplementary data is available at *Cerebral Cortex* online.

Funding

Data used in the preparation of this article were obtained from the Alzheimer's Disease Neuroimaging Initiative (ADNI). Data collection and sharing of ADNI was funded by the National Institutes of Health Grant U01 AG024904 and Department of Defense award number W81XWH-12–2-0012. ADNI is funded by the National Institute on Aging, the National Institute of Biomedical Imaging and Bioengineering, and through generous contributions from the following: Alzheimer's Association; Alzheimer's Drug Discovery Foundation; BioClinica, Inc.; Biogen Idec Inc.; Bristol-Myers Squibb Company; Eisai Inc.; Elan Pharmaceuticals, Inc.; Eli Lilly and Company; F. Hoffmann-La Roche Ltd and its affiliated company Genentech, Inc.; GE Healthcare; Innogenetics, N.V.; IXICO Ltd.; Janssen Alzheimer Immunotherapy Research & Development, LLC.; Johnson & Johnson Pharmaceutical Research & Development LLC.; Medpace, Inc.; Merck & Co., Inc.; Meso Scale Diagnostics, LLC.; NeuroRx Research; Novartis Pharmaceuticals Corporation; Pfizer Inc.; Piramal Imaging; Servier; Synarc Inc.; and Takeda Pharmaceutical Company. The Canadian Institutes of Health Research is providing funds to support ADNI clinical sites in Canada. Private sector contributions are facilitated by the Foundation for the National Institutes of Health (www.fnih.org). The grantee organization is the Northern California Institute for Research and Education, and the study is coordinated by the Alzheimer's Disease Cooperative Study at the University of California, San Diego. ADNI data are disseminated by the Laboratory for Neuro Imaging at the University of California, Los Angeles. This study was supported by the European Research Council, the Swedish Research Council, The Swedish Alzheimer Foundation, the Swedish Brain Foundation, the Marianne and Marcus Wallenberg Foundation, Swedish Foundation for Strategic Research (SSF), the Strategic Research Programme in Neuroscience at Karolinska Institutet (StratNeuro), Hjärnfonden, Birgitta och Sten Westerberg, the Åke Wiberg Foundation and the Swedish Federal Government under the ALF Agreement. The funding sources had no role in the design and conduct of the study; in the collection, analysis, interpretation of the data; or in the preparation, review, or approval of the manuscript .

Notes

Conflict of Interest: None declared.

References

Bassett DS, Bullmore E, Verchinski BA, Mattay VS, Weinberger DR, Meyer-Lindenberg A. 2008. Hierarchical organization of human cortical networks in health and schizophrenia. J Neurosci. 28:9239–9248.

Benjamini Y, Hochberg Y. 1995. Controlling the false discovery rate: a practical and powerful approach to multiple testing. J R Stat Soc Series B. 1:289–300.

Blennow K, Mattsson N, Scholl M, Hansson O, Zetterberg H. 2015. Amyloid biomarkers in alzheimer's disease. Trends Pharm Sci. 36:297–309.

Braak H, Braak E. 1991. Neuropathological stageing of alzheimer-related changes. Acta Neuropathol. 82:239–259.

Buckner RL, Andrews-Hanna JR, Schacter DL. 2008. The brain's default network: anatomy, function, and relevance to disease. Ann NY Acad Sci. 1124:1–38.

Buckner RL, Sepulcre J, Talukdar T, Krienen FM, Liu H, Hedden T, Andrews-Hanna JR, Sperling RA, Johnson KA. 2009. Cortical hubs revealed by intrinsic functional connectivity: mapping, assessment of stability, and relation to alzheimer's disease. J Neurosci. 29:1860–1873.

Buckner RL, Snyder AZ, Shannon BJ, LaRossa G, Sachs R, Fotenos AF, Sheline YI, Klunk WE, Mathis CA, Morris JC, et al. 2005. Molecular, structural, and functional characterization of alzheimer's disease: evidence for a relationship between default activity, amyloid, and memory. J Neurosci. 25:7709–7717.

Bullmore E, Sporns O. 2009. Complex brain networks: graph theoretical analysis of structural and functional systems. Nat Rev Neurosci. 10:186–198.

Chételat G. 2013. Alzheimer disease: Aβ-independent processes—rethinking preclinical AD. Nat Rev Neurol. 9:123–124.

Dennis EL, Thompson PM. 2014. Functional brain connectivity using fMRI in aging and Alzheimer's disease. Neuropsychol Rev. 24:49–62.

Desikan RS, Segonne F, Fischl B, Quinn BT, Dickerson BC, Blacker D, Buckner RL, Dale AM, Maguire RP, Hyman BT, et al. 2006. An automated labeling system for subdividing the human cerebral cortex on MRI scans into gyral based regions of interest. Neuroimage. 31:968–980.

Duan H, Jiang J, Xu J, Zhou H, Huang Z, Yu Z, Yan Z, Alzheimer's Disease Neuroimaging Initiative. 2017. Differences in abeta brain networks in alzheimer's disease and healthy controls. Brain Res. 1655:77–89.

Fagan AM, Mintun MA, Shah AR, Aldea P, Roe CM, Mach RH, Marcus D, Morris JC, Holtzman DM. 2009. Cerebrospinal fluid tau and ptau181 increase with cortical amyloid deposition in cognitively normal individuals: implications for future clinical trials of Alzheimer's disease. EMBO Mol Med. 1: 371–380.

Fischl B, Salat DH, Busa E, Albert M, Dieterich M, Haselgrove C, Van Der Kouwe A, Killiany R, Kennedy D, Klaveness S, et al. 2002. Whole brain segmentation: Automated labeling of neuroanatomical structures in the human brain. Neuron. 33: 341–355.

Forsberg A, Engler H, Almkvist O, Blomquist G, Hagman G, Wall A, Ringheim A, Långström B, Nordberg A. 2008. PET imaging of amyloid deposition in patients with mild cognitive impairment. Neurobiol Aging. 29:1456–1465.

Greicius MD, Krasnow B, Reiss AL, Menon V. 2004. Functional connectivity in the resting brain: a network analysis of the default mode hypothesis. Proc Nat Acad Sci USA. 100:253–258.

Grimmer T, Riemenschneider M, Forstl H, Henriksen G, Klunk WE, Mathis CA, Shiga T, Wester HJ, Kurz A, Drzezga A. 2009. Beta amyloid in alzheimer's disease: Increased deposition in brain is reflected in reduced concentration in cerebrospinal fluid. Biol Psychiatry. 65:927–934.

He Y, Chen ZJ, Evans AC. 2007. Small-world anatomical networks in the human brain revealed by cortical thickness from MRI. Cereb Cortex. 17:2407–2419.

He Y, Chen Z, Evans A. 2008. Structural insights into aberrant topological patterns of large-scale cortical networks in alzheimer's disease. J Neurosci. 28:4756–4766.

Jack CR, Knopman DS, Jagust WJ, Shaw LM, Aisen PS, Weiner MW, Petersen RC, Trojanowski JQ. 2010. Hypothetical model of dynamic biomarkers of the Alzheimer's pathological cascade. Lancet Neurol. 9(1):119–128.

Jack CR Jr, Knopman DS, Jagust WJ, Petersen RC, Weiner MW, Aisen PS, Shaw LM, Vemuri P, Wiste HJ, Weigand SD, et al. 2013. Tracking pathophysiological processes in alzheimer's disease: an updated hypothetical model of dynamic biomarkers. Lancet Neurol. 12:207–216.

Jagust WJ, Landau SM. 2012. Apolipoprotein E, not fibrillar β-amyloid, reduces cerebral glucose metabolism in normal aging. J Neurosci. 32:18227–18233.

Jagust WJ, Landau SM, Shaw LM, Trojanowski JQ, Koeppe RA, Reiman EM, Foster NL, Petersen RC, Weiner MW, Price JC, et al. 2009. Relationships between biomarkers in aging and dementia. Neurology. 73:1193–1199.

Jiang J, Duan H, Huang Z, Yu Z, Alzheimer's Disease Neuroimaging Initiative. 2015. Study of amyloid-beta peptide functional brain networks in AD, MCI and HC. Biomed Mater Eng. 26(Suppl 1):S2197–S2205.

Knopman DS, Jack CR, Wiste HJ, Weigand SD, Vemuri P, Lowe VJ, Kantarci K, Gunter JL, Senjem ML, Mielke MM, et al. 2013. Brain injury biomarkers are not dependent on β-amyloid in normal elderly. Ann Neurol. 73:472–480.

Koivunen J, Pirttilä T, Kemppainen N, Aalto S, Herukka SK, Jauhianen AM, Hänninen T, Hallikainen M, Någren K, Rinne JO, et al. 2008. PET amyloid ligand [11C]PIB uptake and cerebrospinal fluid beta-amyloid in mild cognitive impairment. Dement Geriatr Cogn Disord. 26:378–383.

Landau SM, Fero A, Baker SL, Koeppe R, Mintun M, Chen K, Reiman EM, Jagust WJ. 2015. Measurement of longitudinal β-amyloid change with 18F-florbetapir PET and standardized uptake value ratios. J Nucl Med. 56(4):567–574.

Landau SM, Mintun MA, Joshi AD, Koeppe RA, Petersen RC, Aisen PS, Weiner MW, Jagust WJ. 2012. Amyloid deposition, hypometabolism, and longitudinal cognitive decline. Ann Neurol. 72:578–586.

Latora V, Marchiori M. 2001. Efficient behavior of small-world networks. Phys Rev Lett. 87:198701.

Mathis CA, Mason NS, Lopresti BJ, Klunk WE. 2012. Development of positron emission tomography beta-amyloid plaque imaging agents. Semin Nucl Med. 42: 423–432.

Mattsson N, Insel PS, Donohue M, Landau S, Jagust WJ, Shaw LM, Trojanowski JQ, Zetterberg H, Blennow K, Weiner MW, Alzheimer's Disease Neuroimaging Initiative. 2015. Independent information from cerebrospinal fluid amyloid-beta and florbetapir imaging in alzheimer's disease. Brain. 138:772–783.

Mevel K, Chételat G, Eustache F, Desgranges B. 2011. The default mode network in healthy aging and Alzheimer's disease. Int J Alzheimers Dis. 2011:535816.

Mijalkov M, Kakaei E, Pereira JB, Westman E, Volpe G. 2017. BRAPH: a graph theory software for the analysis of brain connectivity. PLoS One. 12:e0178798.

Mormino EC, Kluth JT, Madison CM, Rabinovici GD, Baker SL, Miller BL, Koeppe RA, Mathis CA, Weiner MW, Jagust WJ, Alzheimer's Disease Neuroimaging Initiative. 2009. Episodic memory loss is related to hippocampal-mediated beta-amyloid deposition in elderly subjects. Brain. 132:1310–1323.

Morris JC, Roe CM, Xiong C, Fagan AM, Goate AM, Holtzman DM, Mintun MA. 2010. APOE predicts amyloid-beta but not tau alzheimer pathology in cognitively normal aging. Ann Neurol. 67:122–131.

Musiek ES, Holtzman DM. 2015. Three dimensions of the amyloid hypothesis: time, space and 'wingmen'. Nat Neurosci. 1: 800–806.

Newman MEJ. 2004. Fast algorithm for detecting community structure in networks. Phys Rev E Stat Nonlin Soft Matter Phys. 69:066133.

Okello A, Koivunen J, Edison P, Archer HA, Turkheimer FE, Någren KU, Bullock R, Walker Z, Kennedy A, Fox NC, Rossor MN. 2009. Conversion of amyloid positive and negative MCI to AD over 3 years An 11C-PIB PET study. Neurology. 73: 754–760.

Palmqvist S, Mattsson N, Hansson O, Alzheimer's Disease Neuroimaging Initiative. 2016. Cerebrospinal fluid analysis detects cerebral amyloid-beta accumulation earlier than positron emission tomography. Brain. 139:1226–1236.

Palmqvist S, Schöll M, Strandberg O, Mattsson N, Stomrud E, Zetterberg H, Blennow, the Alzheimer's Disease Neuroimaging Initiative, the Swedish BioFINDER study, Landau S, et al. 2017. Where β-amyloid fibril accumulation begins in Alzheimer's disease and how it affects brain connectivity. Nat Commun. in press.

Palmqvist S, Zetterberg H, Blennow K, Vestberg S, Andreasson U, Brooks DJ, Owenius R, Hägerström D, Wollmer P, Minthon L, et al. 2014. Accuracy of brain amyloid detection in clinical practice using cerebrospinal fluid β-amyloid 42: a cross-validation study against amyloid positron emission tomography. JAMA Neurol. 71(10):1282–1289.

Palmqvist S, Zetterberg H, Mattsson N, Johansson P, Minthon L, Blennow K, Olsson M, Hansson O, Toresson H, Nägga K, et al. 2015. Detailed comparison of amyloid PET and CSF biomarkers for identifying early Alzheimer disease. Neurology. 85(14):1240–1249.

Palop JJ, Mucke L. 2016. Network abnormalities and interneuron dysfunction in alzheimer disease. Nat Rev Neurosci. 17: 777–792.

Pearson RC, Powell TP. 1989. The neuroanatomy of alzheimer's disease. Rev Neurosci. 2:101–122.

Pike KE, Savage G, Villemagne VL, Ng S, Moss SA, Maruff P, Mathis CA, Klunk WE, Masters CL, Rowe CC. 2007. β-amyloid imaging and memory in non-demented individuals: evidence for preclinical Alzheimer's disease. Brain. 130: 2837–2844.

Raichle ME, MacLeod AM, Snyder AZ, Powers WJ, Gusnard DA, Shulman GL. 2001. A default mode of brain function. Proc Nat Acad Sci USA. 98:676–682.

Rubinov M, Sporns O. 2010. Complex network measures of brain connectivity: Uses and interpretations. Neuroimage. 52:1059–1069.

Sepulcre J, Sabuncu MR, Becker A, Sperling R, Johnson KA. 2013. In vivo characterization of the early states of the amyloid-beta network. Brain. 136:2239–2252.

Sepulcre J, Schultz AP, Sabuncu M, Gomez-Isla T, Chhatwal J, Becker A, Sperling R, Johnson KA. 2016. In vivo tau, amyloid, and gray matter profiles in the aging brain. J Neurosci. 36: 7364–7374.

Shaw LM, Vanderstichele H, Knapik-Czajka M, Clark CM, Aisen PS, Petersen RC, Blennow K, Soares H, Simon A, Lewczuk P, Dean R. 2009. Cerebrospinal fluid biomarker signature in alzheimer's disease neuroimaging initiative subjects. Ann Neurol. 65:403–413.

Son SJ, Kim J, Seo J, Lee JM, Park H, ADNI. 2015. Connectivity analysis of normal and mild cognitive impairment patients based on FDG and PiB-PET images. Neurosci Res. 98:50–58.

Sperling RA, LaViolette PS, O'Keefe K, O'Brien J, Rentz DM, Pihlajamaki M, Marshall G, Hyman BT, Selkoe DJ, Hedden T, Buckner RL. 2009. Amyloid deposition is associated with impaired default network function in older persons without dementia. Neuron. 63:178–188.

Thal DR, Rub U, Orantes M, Braak H. 2002. Phases of A beta-deposition in the human brain and its relevance for the development of AD. Neurology. 58:1791–1800.

Tijms BM, Series P, Willshaw DJ, Lawrie SM. 2012. Similarity-based extraction of individual networks from gray matter MRI scans. Cereb Cortex (New York, NY: 1991). 22(7): 1530–1541.

Tijms BM, ten Kate M, Wink AM, Visser PJ, Ecay M, Clerigue M, Estanga A, Sebastian MG, Izagirre A, Villanua J, Lage PM. 2016. Gray matter network disruptions and amyloid beta in cognitively normal adults. Neurobiol Aging. 37:154–160.

Tolboom N, van der Flier WM, Yaqub M, Boellaard R, Verwey NA, Blankenstein MA, Windhorst AD, Scheltens P, Lammertsma AA, van Berckel BN. 2009. Relationship of cerebrospinal fluid markers to 11C-PiB and 18F-FDDNP binding. J Nucl Med. 50:1464–1470.

van den Heuvel MP, Sporns O. 2013. Network hubs in the human brain. Trends Cogn Sci. 17(12):683–696.

Villeneuve S, Rabinovici GD, Cohn-Sheehy BI, Madison C, Ayakta N, Ghosh PM, La Joie R, Arthur-Bentil SK, Vogel JW, Marks SM, Lehmann M. 2015. Existing pittsburgh compound-B positron emission tomography thresholds are too high: Statistical and pathological evaluation. Brain. 138:2020–2033.

Vlassenko AG, Mintun MA, Xiong C, Sheline YI, Goate AM, Benzinger TL, Morris JC. 2011. Amyloid-beta plaque growth in cognitively normal adults: Longitudinal [11C] Pittsburgh compound B data. Ann Neurol. 70:857–861.

Watts DJ, Strogatz SH. 1998. Collective dynamics of 'small-world' networks. Nature. 393:440–442.

Weiner MW, Aisen PS, Jack CR, Jagust WJ, Trojanowski JQ, Shaw L, Saykin AJ, Morris JC, Cairns N, Beckett LA, Toga A. 2010. The Alzheimer's disease neuroimaging initiative: progress report and future plans. Alzheimers Dement. 6:202–211.

Weiner MW, Veitch DP, Aisen PS, Beckett LA, Cairns NJ, Green RC, Harvey D, Jack CR Jr, Jagust W, Morris JC, Petersen RC. 2017. The Alzheimer's Disease Neuroimaging Initiative 3: continued innovation for clinical trial improvement. Alzheimers Dement. 13:561–571.

Zhou J, Gennatas ED, Kramer JH, Miller BL, Seeley WW. 2012. Predicting regional neurodegeneration from the healthy brain functional connectome. Neuron. 73:1216–1227.